JITH 2017
18èmes Journées Internationales de Thermique (JITH 2017)
Monastir (Tunisie), 25 - 27 Octobre 2017

Design and analysis of a heliostat field layout with reduced shading effect in southern Tunisia

Fathia EDDHIBI, Mahmoud BEN AMARA, Moncef BALGHOUTHI and AmenAllah GUIZANI

Research and Technology Center of Energy, Thermal Processes Laboratory, Hammam Lif, B.P. 95, 2050, Tunisia

mahmoud_bamara@webmails.com
balghouthi_moncef@yahoo.fr
guizania177@gmail.com
eddhibifethia@yahoo.fr

Abstract: This paper dealt with the design and the analysis of a preliminary heliostat field layout with reduced optical losses caused by the blocking and shading effects. The developed heliostat field configuration is simulated in a region of southern Tunisia (latitude: 30.25°N, longitude: 9.55°E), the simulation time was chosen to be the two equinoxes and the two solstices. The code is validated according to a ray tracing method.
The developed heliostat field configuration operate with 0% losses due to shadowing effect on March 21st from 11 am to 4 pm, June 21st from 9am to 5 pm, 21st September from 11 am to 4 pm. Even on December, the number of heliostats causing shadow to their neighbors from 10 am to 3 pm is very low.
Keywords: central receiver system, heliostat field, optical efficiency, shading and blocking efficiency

1. Introduction :

The energy demand is increasing in strength over the world, together with economic growth and environmental pollution. Concentrated solar power technologies can generates about 7% of the worldwide electricity demand by 2030 and it may achieve 25% by 2050 [1]. Central receiver technology presents an attractive method to generate an important concentration ratio of a solar radiation and consequently a high temperature (1000°C). A lower density incident radiation is reflected by a high number of reflective surfaces (heliostat) onto a reduced receiver surface located on the top of the tower. Inside the receiver, the high density solar radiation collected is transferred to a heat transfer fluid, which drives a thermodynamic cycle for power generation.
The heliostat field is a very specific distribution of a large number of reflective mirrors; its arrangement should be very precise due mainly to the individual heliostat motion and to the geographical coordinates of the installation. Due to the high number of heliostats, the reflective surface constitutes the major portion of the total cost of the central receiver system CRS [2]. Heliostat field admits a high number of degrees of freedom which cause about 47% of the annual CRS energy losses [3].
A large number of numerical and experimental studies have been performed on CRS; Corey J. Noone et al. [4] have developed a new computationally efficient heliostat field layout model. All optical losses were detailed in this paper; the existing central receiver power plant PS10 was analyzed. Results show that the developed model was able to improve the PS10 efficiency by 0.36% and to reduce the land area by 15.8%.
A new graphical method to generate a no-blocking heliostat field layout was developed by Siala and Elayeb [5]. Based on a simple mathematical method; the designed model of CRS proposed a heliostat field distribution with no blocking due to the emplacement of heliostats in the field.
In the same context, a new code for the design and the analysis of the heliostat field layout was proposed by Xiudong Wei et al. [6] whose aim was the amelioration of the response speed of the design and the optimization of the heliostat field. An improvement of the existing PS10 layout was detailed. Results showed that, in case of an ideal reflective mirror shape and a perfect tracking system, the spherical heliostat field distribution is less efficient than the toroidal one.
A further field generation methodology was proposed by Yao et al. [7] which aims to reach the maximum optical efficiency. In addition to optical interference, the proposed model took into account the economic effect on the heliostat field configuration.
Firstly, Yao et al. developed a calculation model for the mean annual optical efficiency, this model was able to carry out the exact numerical calculation of the heliostat optical efficiency and especially blocking and shading

efficiency. Then, this proposed model was used to develop a new heliostat field layout generation methodology and validated by rearranging the PS10. Simulation results proved that the mean optical efficiency of the rearranged heliostat field was improved by 0.57% comparing to PS10 design.
A recent CRS study, developed by Eddhibi at al. [8], proposed a mathematical method that allowed the reduction of the complexity and the running time of the blocking and shading calculation procedure.
Due to the importance of heliostat field losses on overall power plant efficiency, the aim of this paper is to design and analyze an efficient heliostat field layout with minimum losses due to the shading and blocking effect. Once we estimated the heliostat field characteristics, an optical analysis was necessary to study the behavior of the heliostat field towards the daily sun motion. This calculation process allowed to account for all optical losses affecting the overall field efficiency. The developed heliostat field configuration is simulated in a region of southern Tunisia (latitude: 30.25°N, longitude: 9.55°E) candidate to host a solar tower power plant. The simulation time was chosen to be the two equinoxes and the two solstices. Finally, the developed code was validated by a ray tracing method. The choice of this region was not arbitrary: Tunisian climate offers efficient operating conditions for concentrated solar power plant with a high potential of DNI especially in the south. In addition, Tunisia location is ideal; it offers the possibility to transfer such kind of energy to the European market due to its proximity to Italy [9].

2. Optical performance of central receiver system:

The evaluation of the CRS optical efficiency is a complicated process due to the significant number of heliostats, the individual motion of each heliostat, the distance between the receiver and the mirror field as well as the limited receiver surface compared to the heliostats field. A new model is detailed, which allows for considering all optical losses affecting the overall efficiency of the CRS (attenuation, spillage, cosine, blocking and shading). The instantaneous efficiency is defined as the product of all optical efficiencies [4].

$$\eta = \eta_{cos} \times \eta_{atm} \times \eta_{ref} \times \eta_{sb} \times \eta_{spillage} \quad (1)$$

2.1 Global coordinate system:

The solar coordinate system includes all the geographic coordinates: latitude, longitude, altitude and time. Referring to these details, the sun's position is defined by two angles: azimuth and zenith. The vector sun position is defined by the normalized vector:

$$s = \begin{pmatrix} s_1 \\ s_2 \\ s_3 \end{pmatrix} = \begin{pmatrix} \sin(\alpha) \times \sin(\gamma) \\ \sin(\alpha) \times \cos(\gamma) \\ \cos(\alpha) \end{pmatrix} \quad (2)$$

2.2 Local coordinate system :

The Cartesian coordinates system (3D) is defined as follows: the x-axis is focusing from the west to the east, the y-axis is from the south to the north and the z-axis is from the ground to the sky.
The local coordinate system is represented by the coordinates of each heliostat; the position of the heliostat is defined by its Cartesian coordinates (x, y, z). The distance between a heliostat and the tower is calculated by the equation below.

$$h_{position} = \sqrt{x_h^2 + y_h^2 + z_h^2} \quad (3)$$

The heliostat's altitude is defined by the angle between the horizontal plane passing through the center of the heliostat and the reflected rays:

$$Al_h = \operatorname{atan}\left(\frac{(H_{tower} - z_h)}{h_{position}}\right) \quad (4)$$

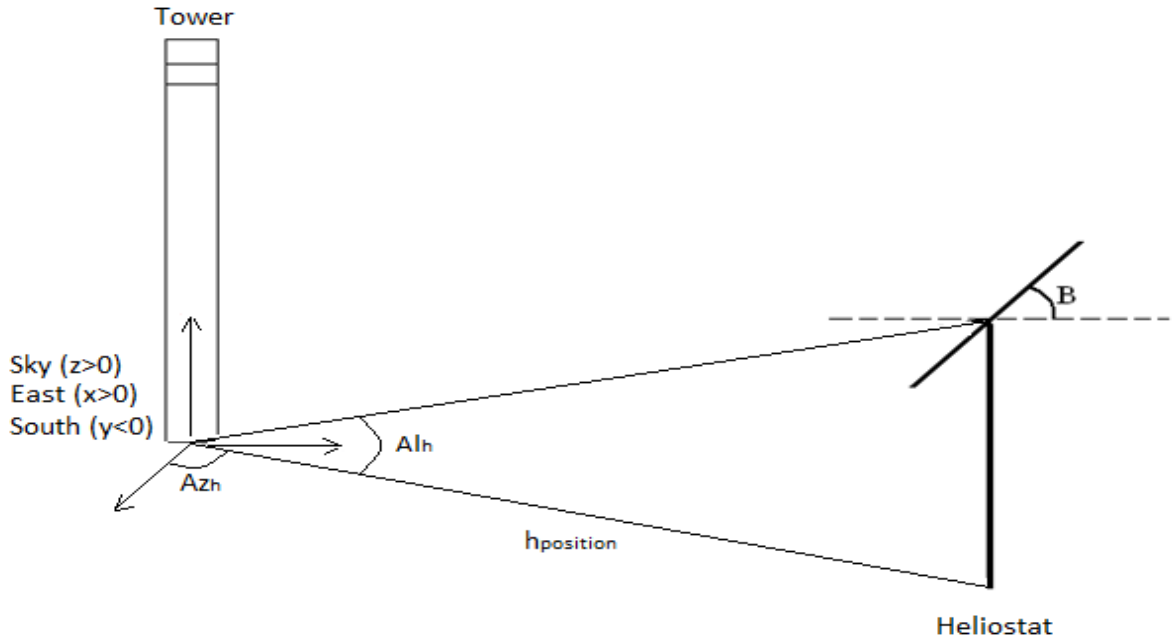

Fig. 1. Local coordinate system

3. Design of heliostat field:

A new code was developed in order to obtain an efficient distribution of a heliostat field with the minimum shading and blocking optical losses. This developed code is a combination between the calculation method validated and published previously by Eddhibi et al. [8] and other published works [5, 6, and 10].
In addition to optical losses, many other conditions should be taken in consideration during the design of the heliostat field layout such as area requirement, accessibility of the operation and maintenance machines…

3.1 Design methodology:

In a first step, radial stagger distribution was chosen as the optimal heliostat field layout as proposed by Collado et al.[10,11] and Siala et al. [5] It is an efficient configuration; it reduces the land consumption and the shading/blocking optical losses. First rows present a high heliostats density contrary to rows located far from the tower, where the spacing between neighboring heliostats increases.
Heliostat field layout is made of circular concentric rows, the optimum first row radius is defined as [12]:

$$R_{min} = 0.8 \times H_t \quad (5)$$

The radial increment was maintained constant, equal to the minimum radial distance between two consecutives rows allowed by mechanical constraints:

$$\Delta R_{min} = D_c \cos 30° \quad (6)$$

Azimuthal spacing is calculated as follow; in 2D, each heliostat is assumed to be circular with a characteristic diameter (Dc) defined as the diagonal of heliostat surface in addition to a separation distance.
The minimum separation distance was defined by Collado et al. [12] as the ratio of the distance between two neighboring heliostats by the heliostat length.

$$s_{min} = 2f - \sqrt{1 + f^2} \quad (7)$$

The second step is the reduction of blocking and shading effect: a previous paper [8] dealt with a new method for the calculation of the blocking efficiencies. The developed method was validated using the PS10 power plant parameters [8]. Starting from this designed heliostat layout, the developed configuration would expand progressively to reduce the blocked/shaded surface.

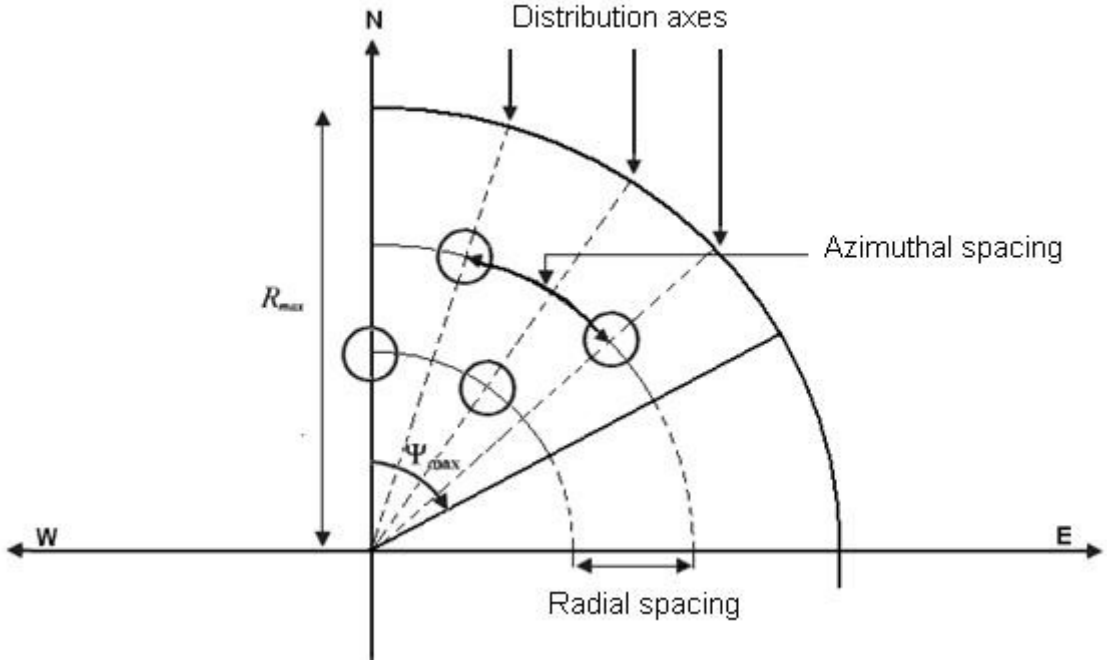

Fig. 2. Basic parameters of heliostat field

Two basics parameters should be considered in this process: the azimuth spacing and the radial distance. The increment of the azimuth spacing is made by the increase of the safety distance between adjacent heliostats. In case of radial distance, the procedure of the heliostat coordinates generation should take into account the spillage losses, atmospheric attenuation and cosine losses. However, once the spacing between heliostats becomes important, additional heliostat can be added.

3.2 Description of the developed configuration:

The heliostat field configuration consists of a central tower surrounded by 3132 heliostats, the field characteristics are detailed in the table below. Heliostats are arranged in 43 rows surrounding the tower. Each row is specified by its number of heliostat, its radial distance as well as the latitude relative to the receiver. In a same row, the heliostats are equidistant.

Figure 3 shows a 2D arrangement of the heliostat field, the coordinates x and y are estimated in meter.

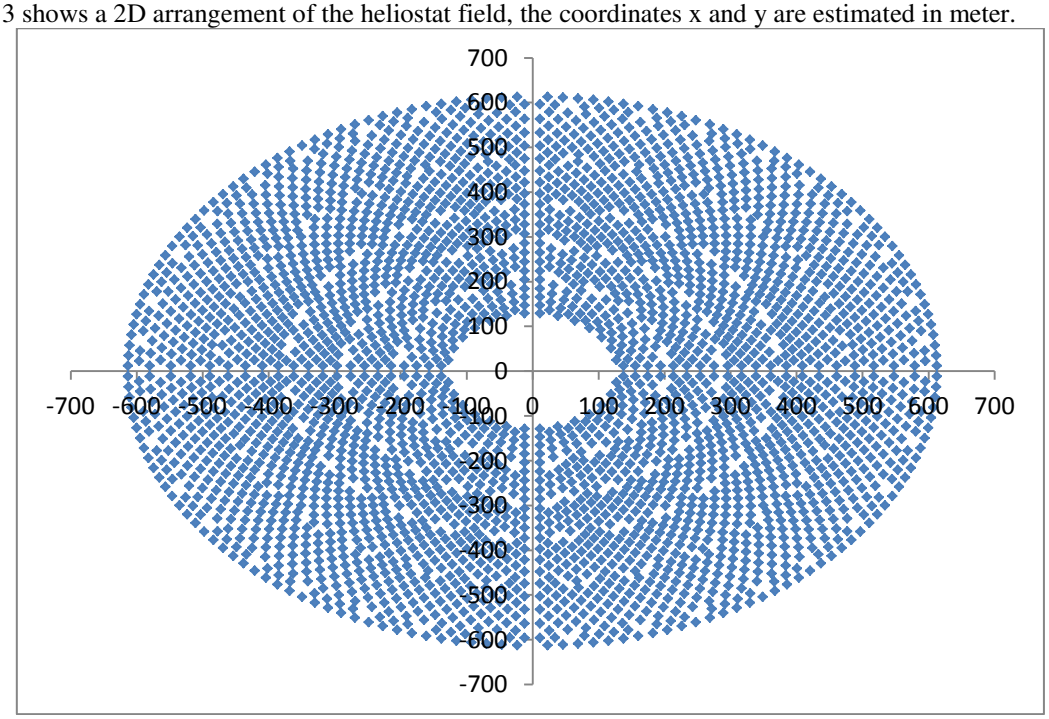

Fig. 3. Heliostat field distribution

Table 1: Characteristics of developed heliostat field.

Total number of heliostats	3132
Heliostat surface [m²]	64
Number of rows	43
Minimum radius of the heliostat field [m]	129.7637
Maximum radius of the heliostat field [m]	613.0768
s_{min} [m]	2

4. Code Validation:

The purpose of this paragraph is to validate the results obtained through the developed optical simulation, designed heliostat field was simulated by ray tracing software and then compared to those obtained by the method we are proposing.

4.1 Ray tracing method:

It is a Monte Carlo ray tracing software for the optical simulation of solar concentrating power systems. Simulation input data are: the collector geometric parameters, the location coordinates (which are useful to calculate the sun position), the number of incident rays, random generation method and the tracking system characteristics. This software is able to quantify every photon launched impinges on a surface and to generates a table made of seven-triples of real numbers in addition to the power per photon. Then, a second computational software is needed to analysis the simulation outputs and to calculate the flow of photons focused on the receiver surface. In addition, an ECMA script code is necessary to introduce the time variation and to reduce the output complexity [13]

Once the configuration of the tower and capture field is developed in 3D, the software is used to simulate the optical behavior of the system under different conditions such as:

- The sun position (elevation, azimuth ...), which defined the direction of the incident solar radiation.
- The direct normal irradiation rates which defined the rate of solar power radiation estimated on a normal surface to the direction of incident solar radiation.

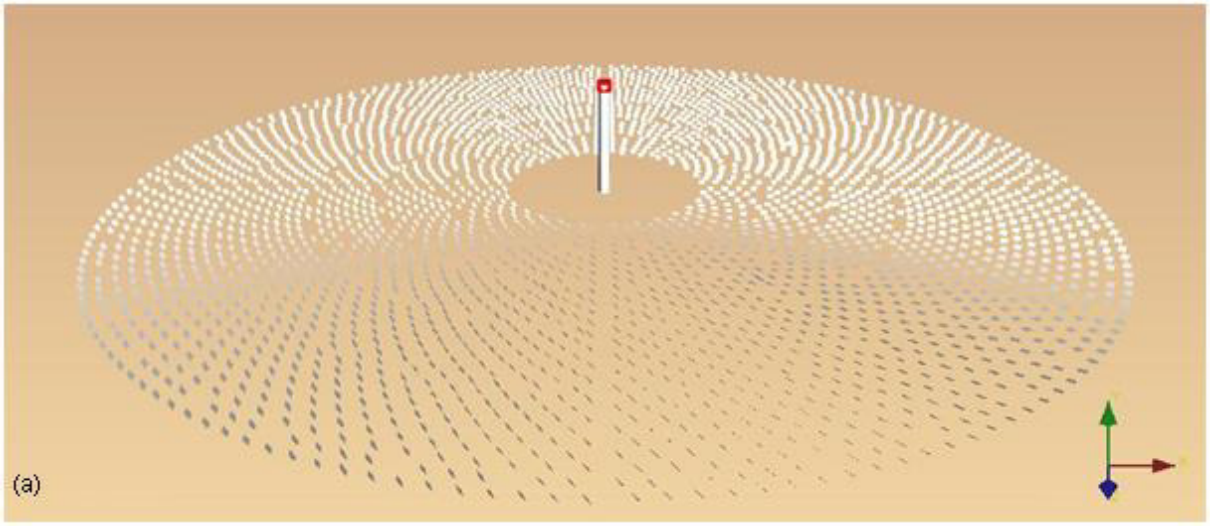

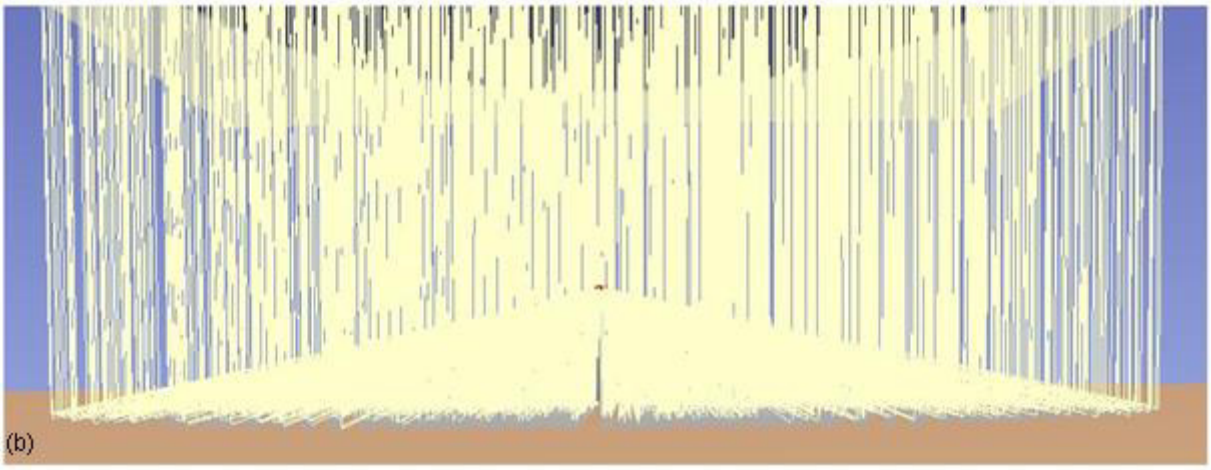

Fig. 4. 3D heliostat field built using ray tracing software

4.2 Validation:

All simulation inputs are assumed to be the same in both methods; the DNI value is fixed to be 1000W/m², the geographical installation coordinates (latitude, longitude) and the simulation date. In both cases, the sun position is estimated by the software itself. In the case of ray tracing method, an ECMA script code was developed to calculate the influence of the sun motion during the day and to reduce the output complexity.

Tables below illustrate the error detected comparing the two simulation process, this error is defined as:

$$e = \frac{\eta_{g,code} - \eta_{g,T}}{\eta_{g,code}} \times 100 \quad (8)$$

Results accessible on the table below present a good agreement between two simulations outputs; the detected error doesn't exceed 6.5%. The analysis of the results proves that, in case of a high incident angle, the detected error is higher. This difference can be due to the fact that ray tracing software generates a random incidence sun light (random generator is Mersenne Twister). Although, in both cases the two calculations procedures were based on the same principle: the heliostat surface reflects the incident rays to the receiver according to the Snell-Descartes Low. The application of this method is different:

In Matlab simulation case, each heliostat corner is projected to the receiver surface, the projected area is assumed to be polygon due to the sun shape.

In ray tracing case, each heliostat is defined by its reflective surface and a tracking system. The tracking system is characterized by its rotation type (the axe of rotation) and the aiming point.

Table 2 : Global optical efficiency comparison, developed code vs ray tracing software

	21st March			21st June			21st Sept			21st Dec		
time	$\eta_{g,code}$	$\eta_{g,T}$	*e%*	$\eta_{g,code}$	$\eta_{g,T}$	*e%*	$\eta_{g,code}$	$\eta_{g,T}$	*e%*	$\eta_{g,code}$	$\eta_{g,T}$	*e%*
7	0.49	0.48	2.02	0.53	0.49	6.08	0.54	0.52	3.39	0.47	0.45	4.98
8	0.49	0.48	3.39	0.57	0.54	5.55	0.57	0.55	1.85	0.47	0.45	4.99
9	0.55	0.54	2.19	0.61	0.61	0.25	0.57	0.56	1.41	0.48	0.46	6.47
10	0.59	0.58	2.49	0.63	0.62	0.69	0.60	0.59	1.70	0.51	0.51	0.77
11	0.62	0.60	1.39	0.65	0.65	0.10	0.62	0.61	0.90	0.52	0.52	0.63
12	0.63	0.61	1.63	0.66	0.66	0.60	0.63	0.62	0.75	0.52	0.52	0.51
13	0.64	0.62	1.05	0.67	0.67	0.07	0.64	0.62	1.56	0.52	0.53	0.07
14	0.64	0.62	1.63	0.67	0.67	0.08	0.64	0.63	0.97	0.52	0.53	0.11
15	0.63	0.61	1.60	0.66	0.66	0.32	0.63	0.61	2.46	0.52	0.51	1.98
16	0.62	0.61	0.34	0.64	0.65	0.98	0.61	0.60	1.64	0.51	0.51	0.09
17	0.59	0.59	1.51	0.63	0.61	2.20	0.59	0.57	2.61	0.47	0.46	3.82
18				0.59	0.57	4.70	0.53	0.52	1.33			
19				0.5	0.50	3.07						

5. Optical heliostat field efficiency:

The heliostat field optical efficiency depends on the daily sun motion as well as the variation of sun height from one season to another.

5.1 average daily shading and blocking efficiency analysis:

A detailed analysis of all optical losses that arise due to motion of the heliostat tracking system from sunrise to sunset is developed. To ensure the consideration of all these parameters, the time of the simulation is chosen to be March 21st, June 21st, September 21st and December 21st. The developed heliostat field configuration is simulated in a region of southern Tunisia (latitude: 30.25°N, longitude: 9.55°E). The simulation time step is chosen to be 1 hour, consequently the daily average optical efficiency is calculated as follows:

$$\eta_{opt} = \frac{\Sigma \eta_{ins}}{\text{Number of iteration}} \quad (9)$$

The detailed analysis of optical losses is a delicate process due to the large number of variables such as the number of reflective mirrors, heliostat coordinates, sun position….

The developed method aims to create an efficient heliostats field distribution with a minimum shading and blocking losses. The calculation method of the blocking/shading method is summarized in the organization chart below. The value of the shading/ blocking efficiency is defined as follow:

$$\eta_{Blo} = 1 - \frac{S_{bloc}}{S_{hel}} \quad (10)$$

$$\eta_{Shad} = 1 - \frac{S_{shad}}{S_{hel}} \quad (11)$$

The analysis of the shading effect shows that the heliostat field is highly efficient; the shading efficiency varies from 0.952 to 1. This means that the shaded areas are reduced and they may reach the zero value.

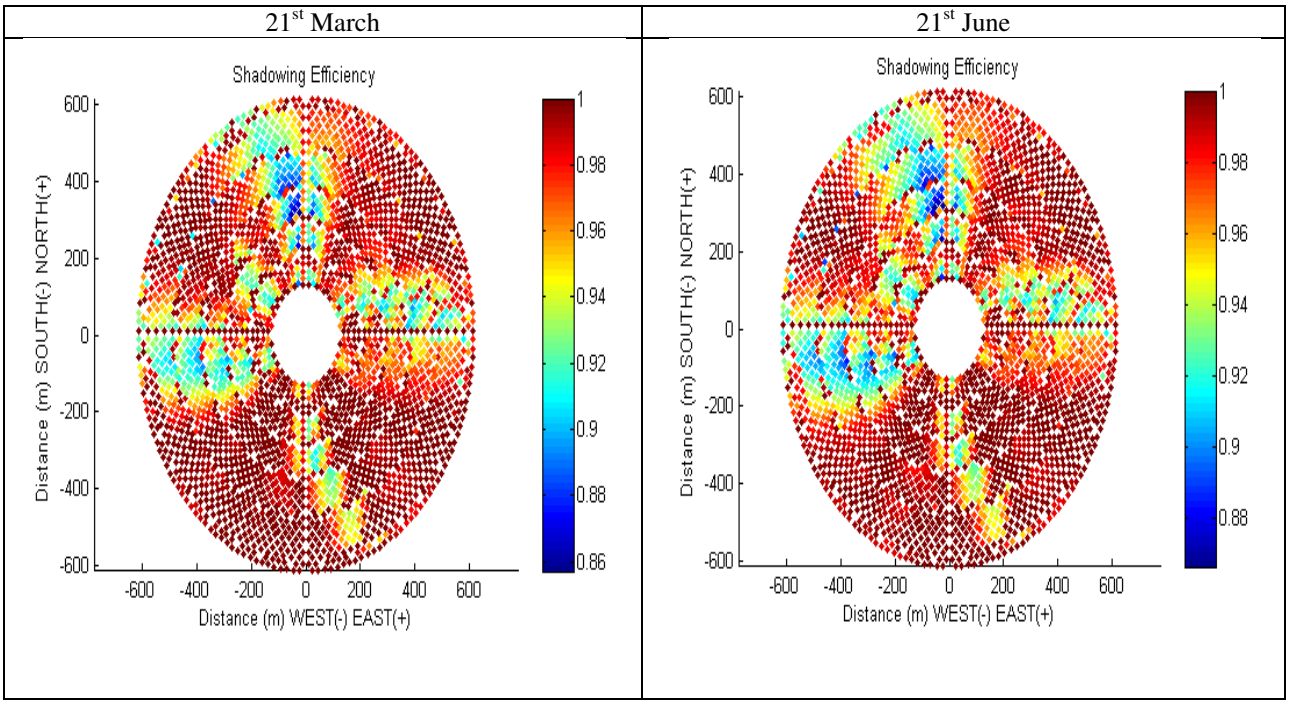

Fig. 5. Distribution map of the daily average shading efficiency for March 21st and June 21st

Simulation results prove that the daily average shading effect is low in June 21st compared to values obtained on March 21st. Although this variation is relatively small (0.01), the heliostat field configuration can be considered more profitable during summer.

As regards the blocking losses, only the North area of the developed configuration is affected by this type of loss. In the first case (21st March), blocking efficiency is in the ranges is of 0.395 to 1. The heliostats located in the southern part of the field track the sun motion without generating the blocking effect to their neighbors. The results of the simulation of June 21st show that the blocking efficiency varies between 0.428 and 1.

21st March	21st June

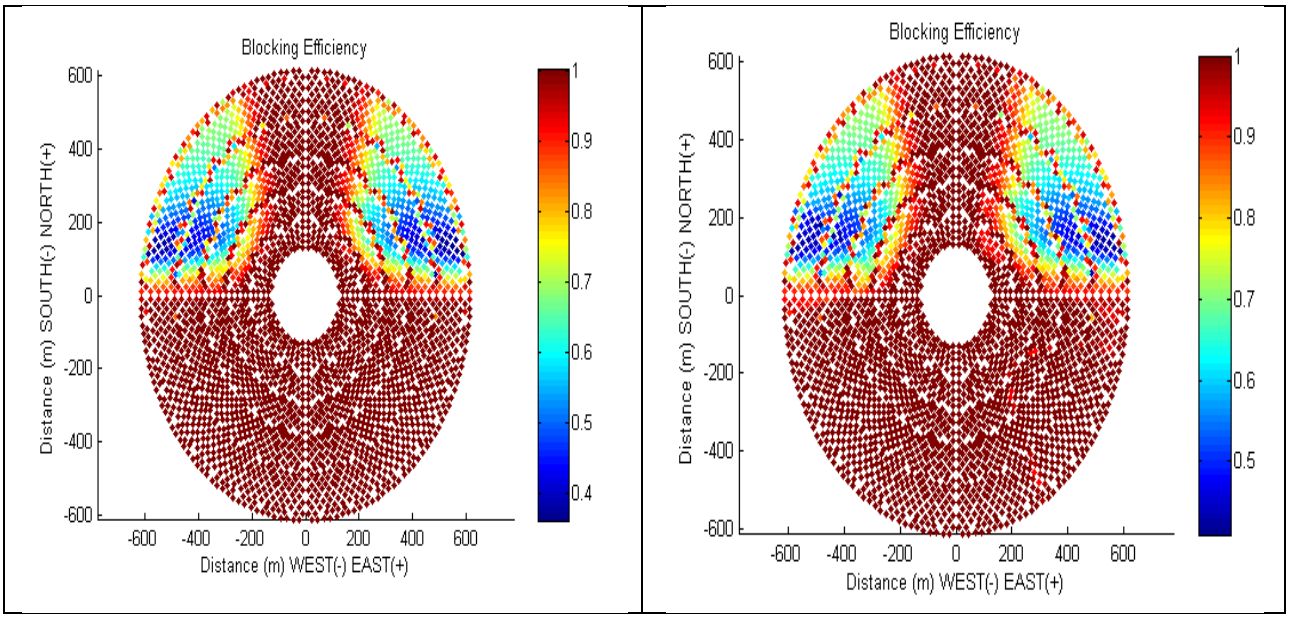

Fig. 6. Distribution map of the daily average blocking efficiency for March 21st and June 21st

5.2 Hourly shading and blocking efficiency analysis:

In the previous step, each simulation generates the daily average of 5 types of optical losses. Therefore, reducing the step time, the number of sunny hours and the seasonal variation amplify the quantity of results. To reduce this complexity, only a few significant hours of the day (morning, noon, afternoon) will be analyzed in this section.

A detailed analysis of heliostats behavior throughout the day proves that the developed distribution of reflective mirrors minimizes the effect of blocking and shading optical losses.

Figure 19 shows that at low incidence angle, the field operates with 0% shading losses. On March, June and September, the simulation results prove that there is no detection of heliostats that cause shadow to their neighbors.

Similarly for blocking, the number of heliostats causing the blocking effect is low on 21st June, it does not exceed 200 heliostats.

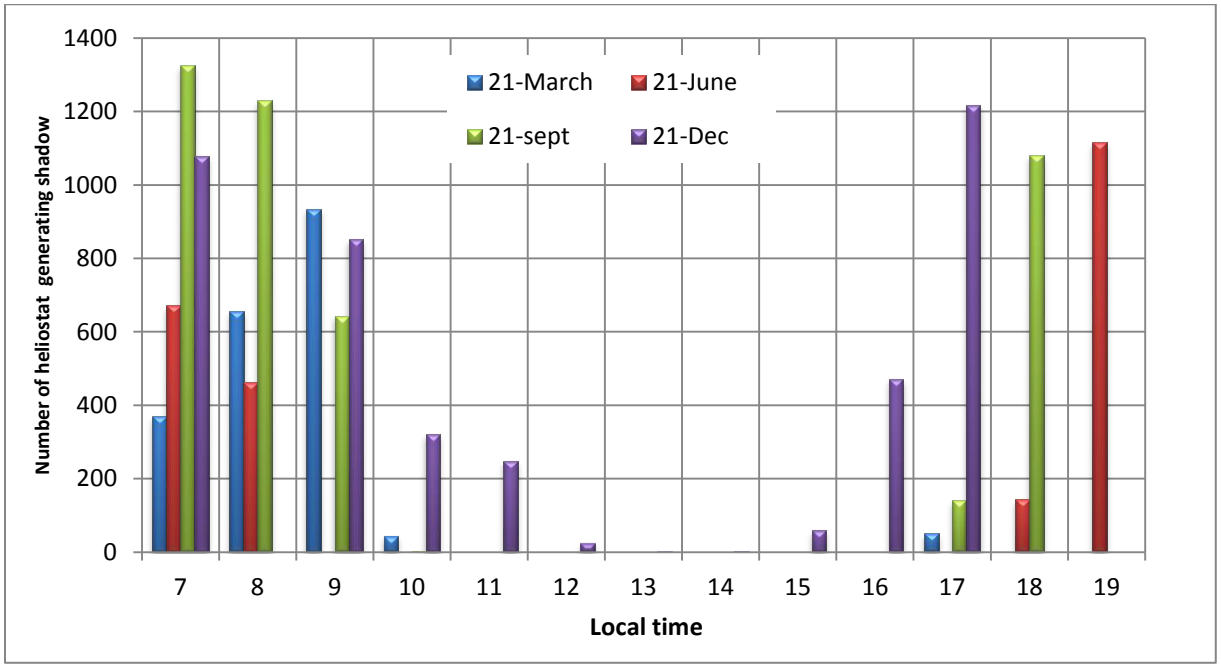

Fig. 7. Number of heliostat generating shading to their neighbor

On the contrary, on December the number of heliostats subject the blocking effect is high, it can exceed 2 400 heliostats. The calculation process is iterative; the number of heliostats obtained is the sum of all cases detected along the day.

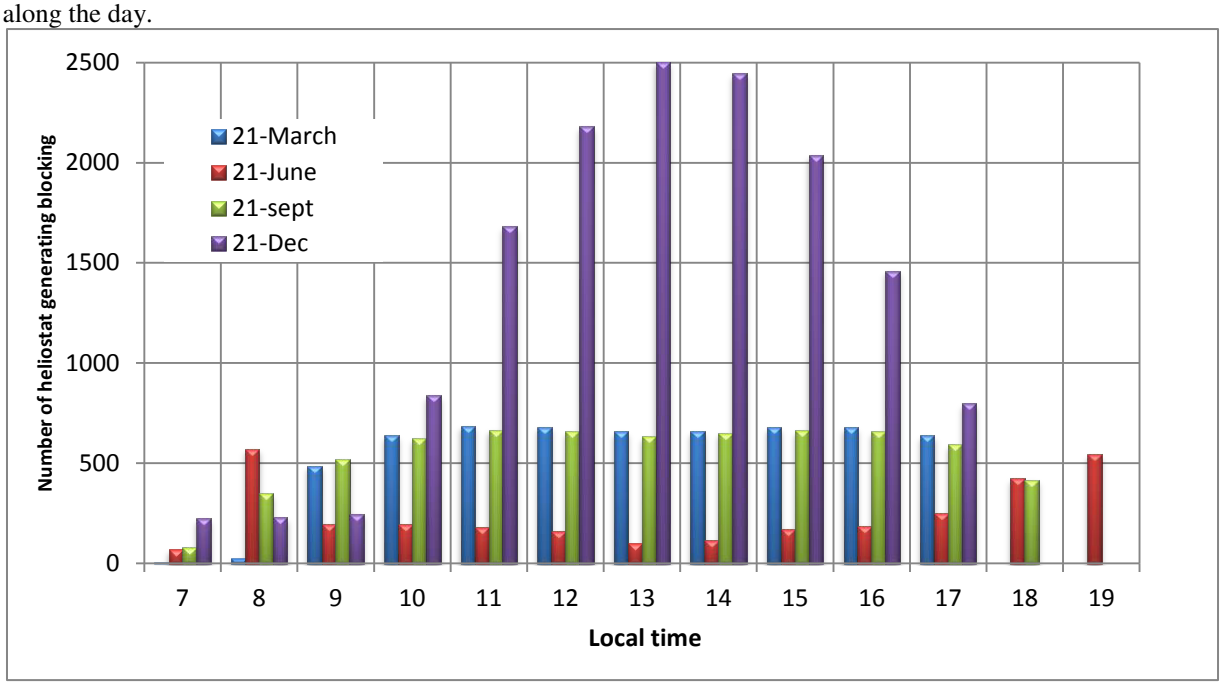

Fig. 8. Number of heliostat generating blocking to their neighbor

December 21st at 8 am, the sun elevation is low. The developed model has not detected any case of blockage. Similarly to March 21st, the number of heliostats causing the blocking effect is small with reduced blocked surfaces.

On September and June, at 8am, the incident rays reach the heliostats with a high angle of incidence. To obey the law of Snell -Descartes, the heliostat inclination angle must be low, which improve the blocking phenomenon.

June 21st, only the southern part of the heliostat field is affected by the blockage. All heliostats of the northern region admit a significant tilt angle. In this region, the blocking rate is zero, the blocking efficiency is 1.

21st March	21st June
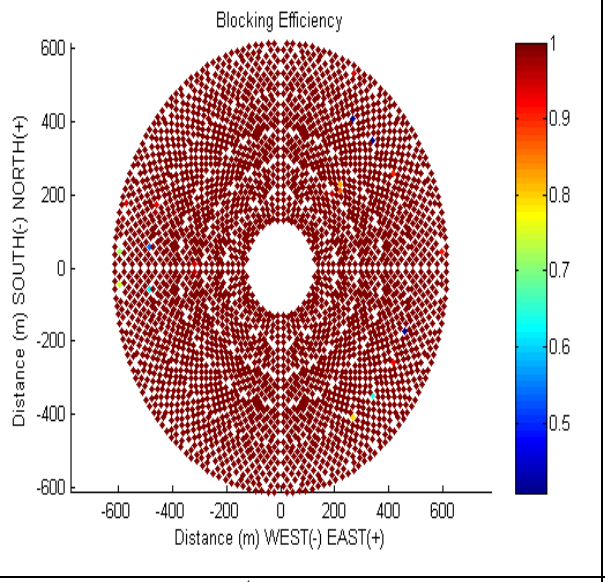	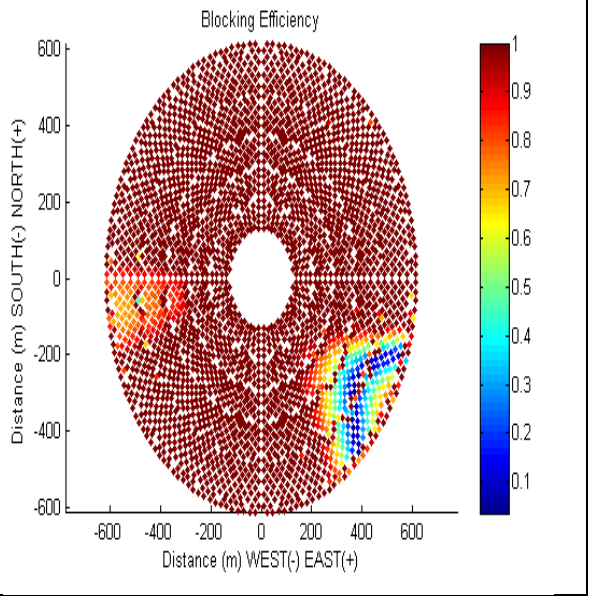
21st September	

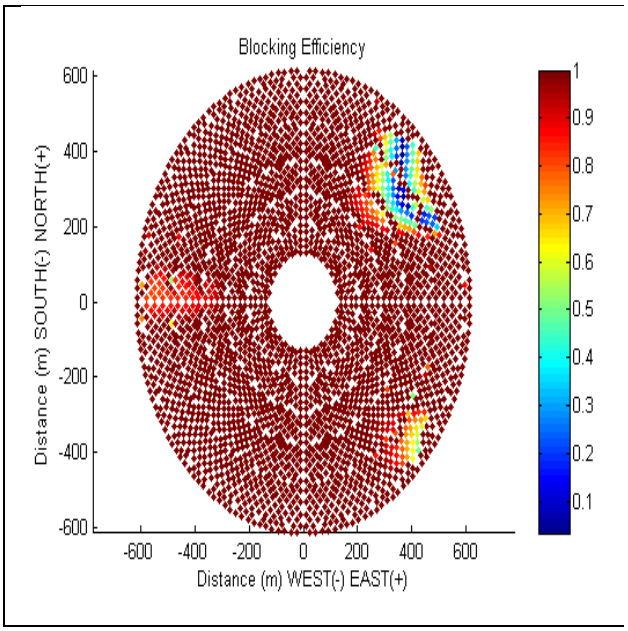

Fig. 9. Distribution map of the hourly average blocking efficiency at 8 am

The comparison between the distributions of the blocking efficiency illustrated below shows the effect of the sun height on the phenomenon of blocking. On June 21st, the sun is higher than other days, which proves the low optical loss by blocking effect. In December, the sun height is low. The sun is always in the southern region, the northern heliostat field part is affected by blocking with values ranging from 0.063 to 0.674.

21st March	21st June
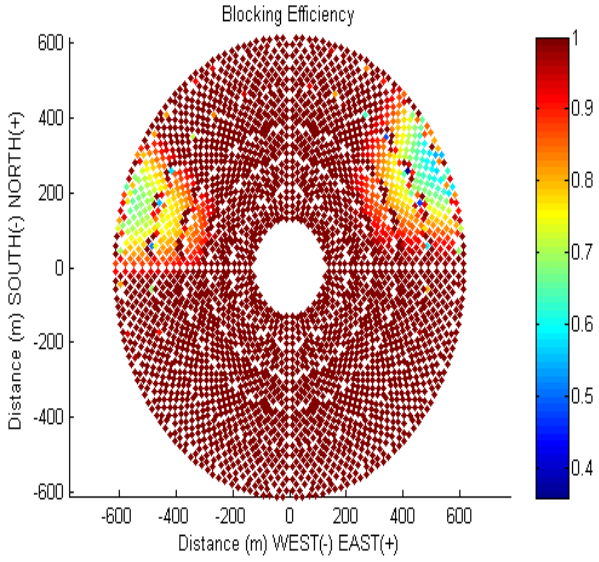	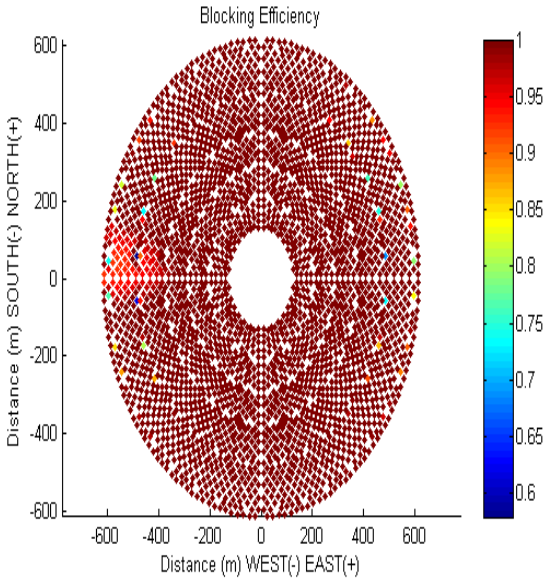
21st September	21st December

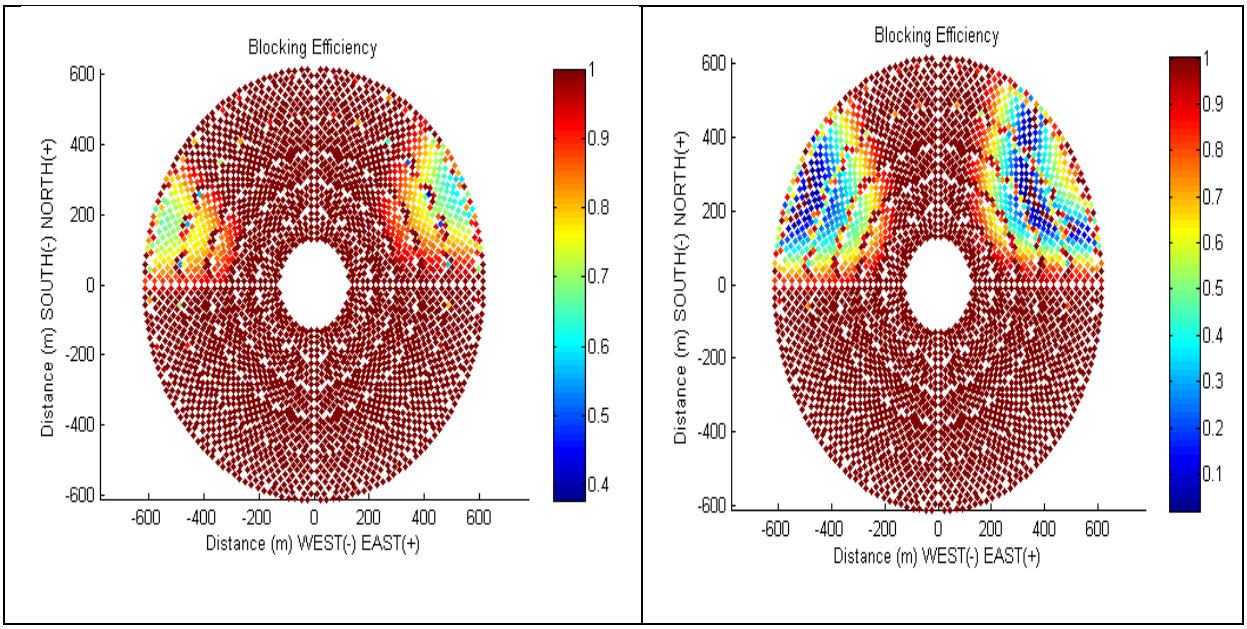

Fig. 10. Distribution map of the hourly average blocking efficiency at noon

During March and September, the sun height variation is insignificant in the considered region which generates two comparable distributions.

In the afternoon, the sun is located on the south west region of the heliostat field.

June 21st, the blocking efficiency is low with values higher than 0.8. The blocking loss distribution is spread over a reduced portion of the field; the number of heliostats affected by blocking is low.

21st March	21st June
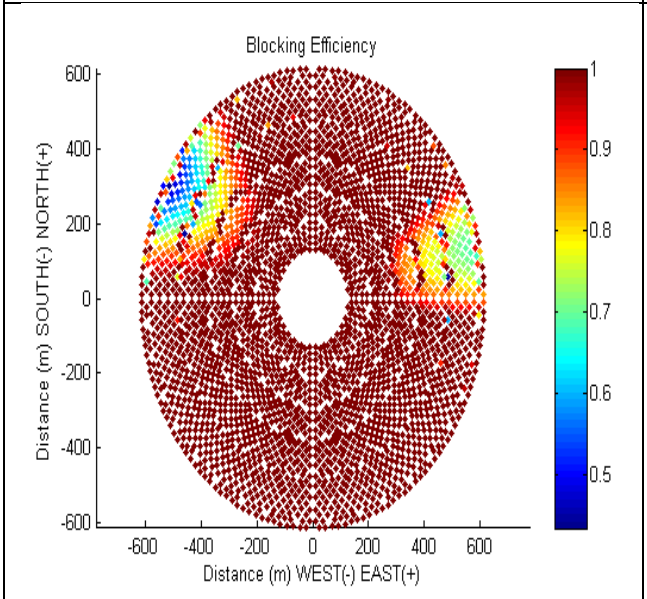	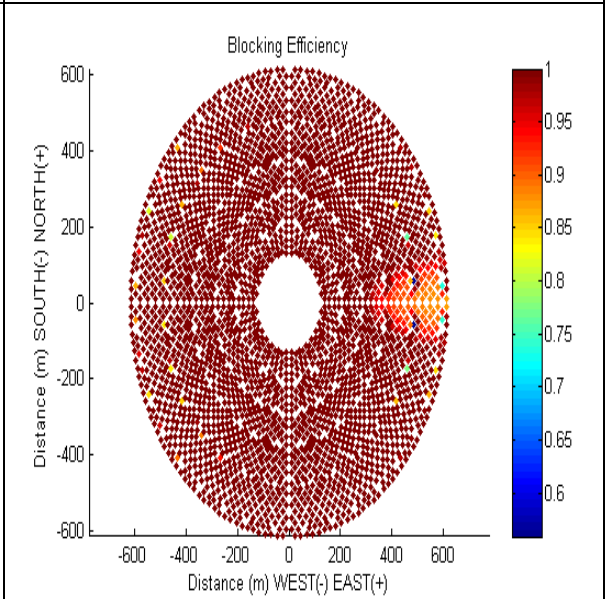
21st September	21st December

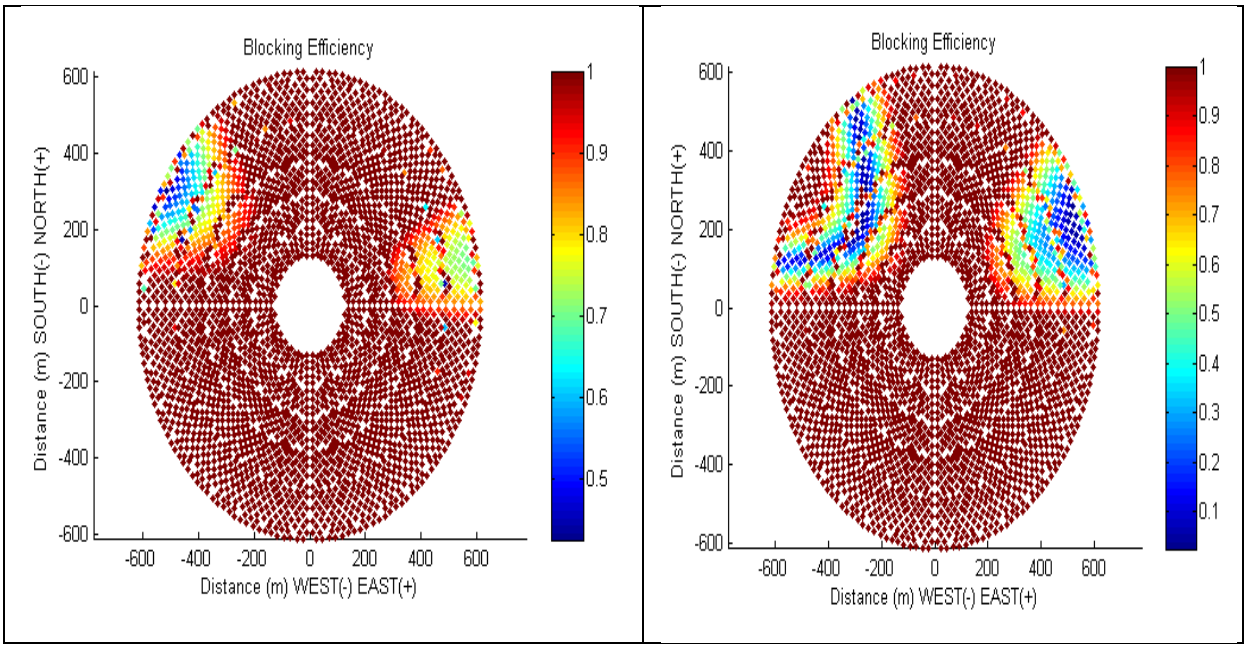

Fig. 11. Distribution map of the hourly average blocking efficiency at 4 pm

Simulation results show that the developed heliostat field configuration managed to operate successfully with 0% losses by shadowing effect for March 21st from 11 am to 4 pm, for June 21st from 9 am to 5 pm, for 21st September from 11 am to 4 pm. Even on December, the number of heliostats causing shadow to their neighbors from 10 am to 3 pm is very low, and is inferior to 321.

Results of this simulation are detailed below; at 8am, the sun is in the east with low elevation. The western part of the field is affected by shadowing, except for December 21st, no cases are detected. June 21st, the shading efficiency is greater than 0.672, and is enhanced on March 21st until 0.278.

21st March	21st June
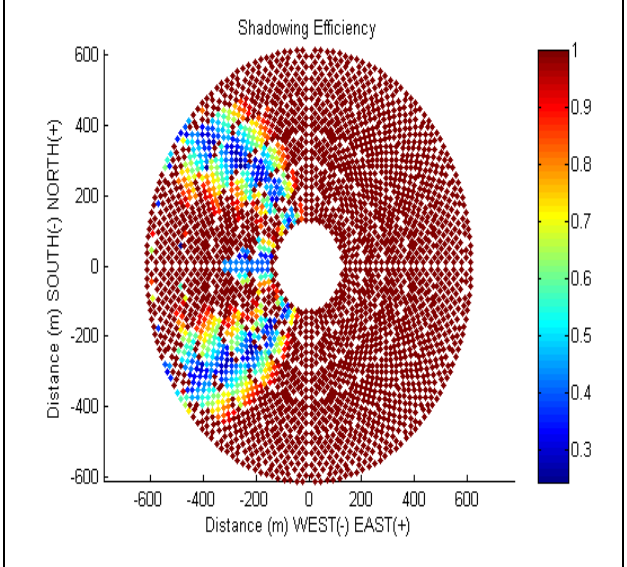	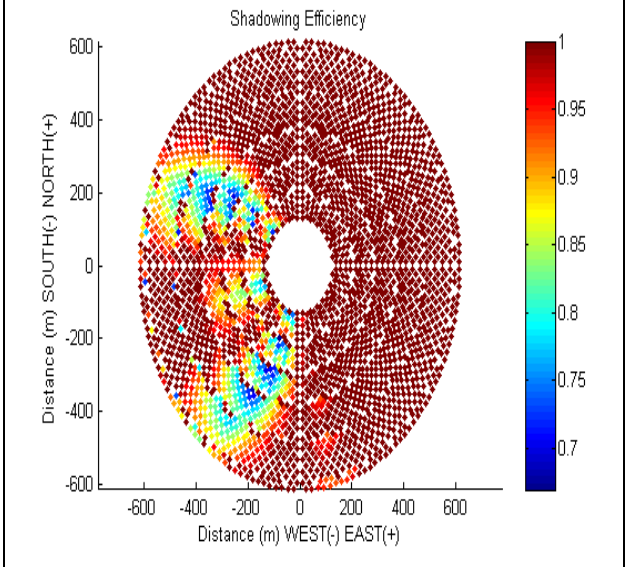
21st September	

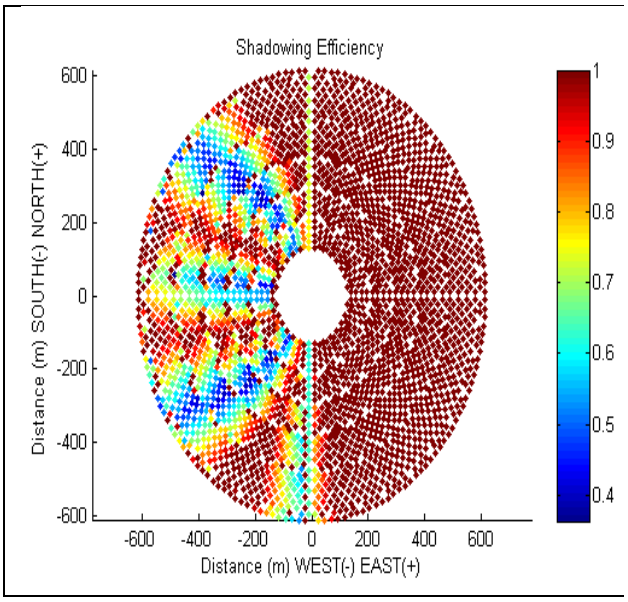

Fig. 12. Distribution map of the hourly average blocking efficiency at 8 am

At noon, the field configuration is reliable; the heliostats track the sun motion and focus incident ray on the receiver surface without generating the shadow to their neighbors. In the case of 21st December, only 25 heliostats were detected with a shading efficiency higher than 0.988.

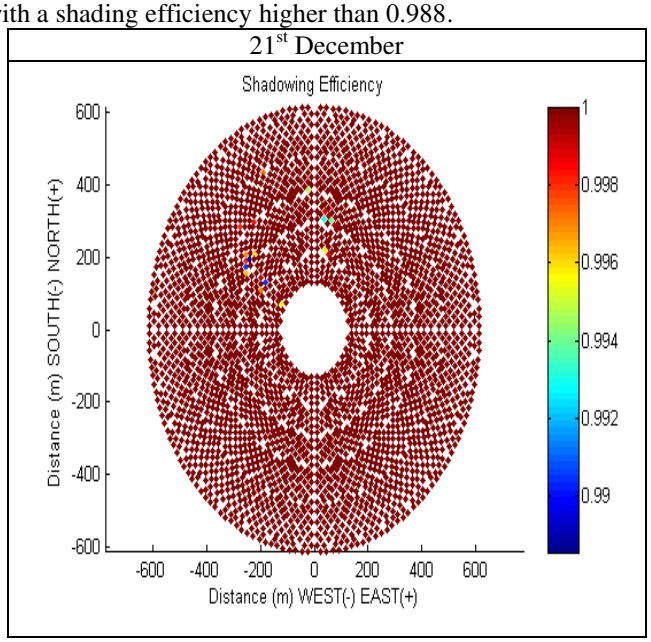

Fig. 13. Distribution map of the hourly average shading efficiency at noon

In the afternoon, the efficiency is increasing but it is still weak. It varies between 0.80 and 1 (Fig. 26).

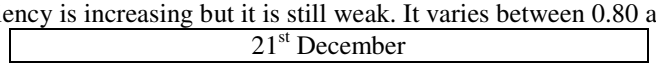

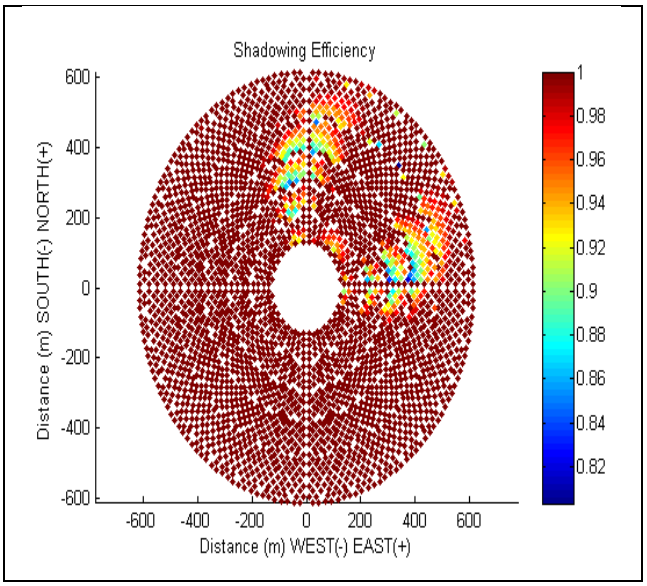

Fig. 14. Distribution map of the hourly average shading efficiency at 4 pm

6. Conclusion:

In this paper, a new code for the design and the analysis of a heliostat field layout was developed.

With reference to a previous work, a method recently validated using the PS10 database, an efficient heliostat field configuration was designed with the aim of reducing optical losses due to the blocking and shading. The new configuration is made of a cylindrical tower, surrounded by 3132 heliostats arranged in 43 rows.

In a second step, the optical analysis of the new developed configuration was necessary to study shading and blocking optical losses. The average daily analysis showed that the comparison between different simulation results (21st March, 21st June, 21st September and 21st December) didn't present a significant variation; the difference was within an accuracy of +/-0.01.

A detailed analysis of heliostats behavior throughout the day proves that the developed heliostat field minimizes the effect of blocking and shading optical losses. On March, June and September, the simulation results prove that there is no detection of heliostats that cause shadow to their neighbors. Similarly for blocking, the number of heliostats causing the blocking effect is low on 21st June, it does not exceed 200 heliostats.

The simulation results show that the developed heliostat field configuration managed to operate successfully with 0% losses by shadowing effect on March 21st from 11 am to 4 pm, June 21st from 9 am to 5 pm, 21st September from 11 am to 4 pm. Even on December the number of heliostats causing shadow to their neighbors from 10am to 15h is very low, inferior than 321.

This paper can be a preliminary study of solar tower power plant in the region of southern Tunisia.

References:

[1] Ziuku S, Seyitini L, Mapurisa B, Chikodzi D, Koen V K. Potential of Concentrated Solar Power (CSP) in Zimbabwe. Energy for Sustainable Development, Volume 23, 220–227, 2014.

[2] Kolb GJ, Jones SA, Donelly MW, Gorman D, Thomas R, Davenport R, et al. Heliostat cost reduction study, SAND2007-3293, 2007.

[3] William B S, Micheal G. Power from the sun 2001.
Available from: <http://www.powerfromthesun.net/book.htm>.

[4] Noone CJ, Torrilhon M, Mitsos A. Heliostat field optimization: A new computationally efficient model and biomimetic layout. Solar Energy, Volume 86, 792–803, 2012.

[5] Siala FMF, Elayeb ME. Mathematical formulation of a graphical method for a no-blocking heliostat field layout. Renewable Energy, Volume 23, 77–92, 2001.

[6] Xiudong W, Zhenwu L, Weixing Y, Zhifeng W. A new code for the design and analysis of the heliostat field layout for power tower system. Solar Energy, Volume 84, 685–690, 2010.

[7] Yingxue Y, Yeguang H, Shengdong G. Heliostat field layout methodology in central receiver systems based on efficiency-related distribution. Solar Energy, Volume 117, 114–124, 2015.

[8] Eddhibi F, Ben Amara M, Balghouthi M, Guizani A. Optical study of solar tower power plants. Journal of Physics: Conference Series, Volume 596, 012018, 2015.

[9] Balghouthi M, Trabelsi SE, Ben Amara M, Bel Hadj Ali A, Guizani A. Potential of concentrating solar power (CSP) technology in Tunisia and the possibility of interconnection with Europe. Renewable and Sustainable Energy Reviews, Volume 56, 1227–48, 2016.
[10] Collado FJ. Preliminary design of surrounding heliostat fields. Renewable Energy, Volume 34, 1359-63, 2009.
[11] Collado FJ, Guallar J. Campo: Generation of regular heliostat fields. Renewable Energy, Volume 46, 49-59, 2012.
[12] Collado FJ , Turégano JA.. Calculation of the annual thermal energy supplied by a defined heliostat field. Solar Energy, 42, 149–65, 1989.
[13] ECMAScript Language specification, 5.1 Edition/ June 2011 http://www.ecma-international.org
[14] Schmitz M, Schwarzbölz P, Buck R, Pitz-Paal R. Assessment of the potential improvement due to multiple apertures to central receiver systems with secondary concentrators. Solar Energy, Volume 80,111–20, 2006.

Nomenclature

s	sun position vector, *m*
Al_h	heliostat altitude, °
Az_{hel}	heliostat azimuth, °
$h_{position}$	heliostat position, *m*
H_{tower}	tower height, *m*
B	angle of inclination, °
$dist$	distance between the tower and the heliostat, *m*
DNI	Direct Normal Irradiation
N	photon number
CRS	central receiver system
R	distance between the tower and the row, *m*
R_{min}	first row radius, *m*
H_t	height of the aiming point, *m*
D_c	characteristic diameter, *m*
D	heliostat diagonal, *m*
s_{min}	minimum additional separation distance, *m*
f	heliostat width to length ratio
S_{Sp}	Spilled surface, m^2
S_{bloc}	Blocked surface, m^2
S_{shad}	Shaded surface, m^2
S_{hel}	Heliostat surface, m^2
η_{cos}	cosine efficiency
η_{atm}	atmospheric attenuation efficiency
η_{opt}	optical efficiency
η_{ref}	reflectivity efficiency
η_{sb}	shading and blocking efficiency
$\eta_{spillage}$	spillage efficiency
η_{ins}	instantaneous efficiency
$\boldsymbol{\eta_{g,code}}$	Global efficiency resulting from developed code
$\boldsymbol{\eta_{g,T}}$	Global efficiency resulting from ray tracing software
θ_i	incident angle, °
α	solar azimuth, °
γ	solar zenith, °